Photorefractive fixing and related thermal effects in $LiNbO_3$

1991 J. Phys.: Condens. Matter 3 5399

(http://iopscience.iop.org/0953-8984/3/28/014)

J. Phys.: Condens. Matter 3 (1991) 5399–5406. Printed in the UK

Photorefractive fixing and related thermal effects in $LiNbO_3$

L Arizmendi, P D Townsend†, M Carrascosa, J Baquedano and J M Cabrera

Física Aplicada C-IV, Universidad Autónoma de Madrid, Cantoblanco, Madrid ES-28049, Spain

Received 3 January 1991, in final form 28 March 1991

Abstract. The thermal and optical stability of photorefractive holograms written in iron-doped $LiNbO_3$ have been measured over the temperature range from 50 to 165 °C. In each case the decay proceeded as a non-simple exponential process exhibiting several more or less resolvable stages. For optically erased holograms the activation energy of the two observed stages was 0.15 ± 0.01 eV. Thermal erasure revealed at least four stages with activation energies ranging from 0.85 to 0.95 eV. Homogeneous illumination at room temperature gave rise to a fixed-developed hologram whose diffracted signal was about 1% of that shown by the initially light-recorded hologram. The developed signal was approximately the same after four successive erasing–developing cycles. Thermal erasure results are interpreted in terms of only proton migration, within the framework of recent models for photorefractive fixing. Thermal electron detrapping proceeds at higher temperatures ($T > 170$ °C) in lightly reduced samples.

1. Introduction

The photorefractive effect has been studied by many groups since the first observation of optical damage in $LiNbO_3$ by Ashkin *et al* (1966). Despite this lengthy period of interest a full understanding of the mechanism is not yet universally agreed. In part this may be that there is not a unique mechanism which operates in all samples, since the photorefractive process is a function of the various defect concentrations within the $LiNbO_3$. Even for idealized 'pure' crystals it should be noted that $LiNbO_3$ is never fully stoichiometric and normal material is grown at the 'congruent' point of the phase diagram. In real (i.e. impure) crystals this offers the possibility of a complex mixture of intrinsic and extrinsic defect interactions. Facts which are generally agreed are the following. Photoexcited carriers migrate under various transport mechanisms and become trapped at different sites. This generates a space-charge field which, via the electro-optic effect, induces a modulation of the refractive index. Above room temperature (RT), field-induced ion migration may occur. A refractive index pattern arising from ionic space-charge field is called a *fixed* pattern.

The individual processes which allow the ion or electron migration to be responsible for photorefraction will be characterized by particular activation energies and pre-exponential factors (i.e. vibrational frequency terms). Hence, plots of diffraction efficiency versus time, under either light or dark conditions, as a function of $1/T$ should

† Permanent address: MAPS, University of Sussex, Brighton BN1 9QH, UK.

0953-8984/91/285399 + 08 $03.50

yield the activation energies of the contributory factors. Previous measurements of this type have led to activation energies near 0.2 eV for optical erasure (Anghert *et al* 1972, Belabaev *et al* 1976, Ohmori *et al* 1976, Barkan *et al* 1980, Balsa and Bobyl 1985), and near 1.0 eV for thermal erasure (Amodei and Staebler 1972a, b, Belabaev *et al* 1976, Pashkov *et al* 1979). Also the thermal dependence of photoconductivity has been measured (Jösch *et al* 1978, Krätzig and Orlowsky 1980). The data obtained lead, as expected from theory (Zylberstejn 1976), to activation energies in the same range as for the data of optical erasure (about 0.2 eV).

Since thermal erasure is closely related to the fixing process, both subjects are frequently considered together. According to the first report of fixing by Amodei and Staebler (1971, 1972a, b), ionic migration takes place at about 150 °C, well below the electron thermal excitation which should occur above 200 °C. Vormann *et al* (1981) have given evidence that protons existing in the lattice are driven by the field of the recorded grating to form a complementary grating that neutralizes the electronic grating.

Hydrogen is known to be present in as-grown pure and doped $LiNbO_3$ in concentrations of 10^{18}–10^{19} cm^{-3} (see, e.g., Kovacs and Fölvari 1989). Measured values of the activation energy for proton migration or electron detrapping are rather scattered (say from 0.5 to 1.4 eV) and there still persist some doubts about whether both processes occur at different or similar temperatures. On the other hand, a theoretical model which assumes a much lower temperature for proton migration than for electron detrapping (Hertel *et al* 1987) predicts an exponential build-up of the protonic grating, whereas a recent improved model (Carrascosa and Agulló-López 1990) takes into account proton–electron competition and predicts non-exponential decays of the refractive index during the fixing process.

This paper presents experimental data on optical and thermal erasure of gratings recorded in $LiNbO_3$ within the 50–165 °C range. In addition to the conventional thermal decays leading to Arrhenius-type data, a new technique has been used which is to make a dynamic measurement of the diffraction efficiency whilst heating the sample at a constant rate. By carrying out these two different types of thermal experiment and by using recent fixing models to interpret the data, a better understanding of the role played by protons and electrons during the fixing process is expected to be gained. Values of activation energies and pre-exponential factors will also be presented and discussed.

2. Experimental details

The study was made with a crystal of $LiNbO_3$ doped with 0.1 wt% Fe. The holographic gratings were written with 514 nm argon laser beams set at an angle of 18° to the crystal surface normal (a grating spacing of 0.83 μm). The ratio of beam powers was about 500:1 (e.g. 105 and 0.2 mW cm^{-2}) since this provides the low modulation depth ($m \simeq 0.1$) required to avoid grating harmonics. The orientation of the crystal was chosen to have the *c* axis in the plane of the sample and parallel to the grating vector. The diffraction efficiency of the grating was monitored by recording the changes in intensity of a low power (approximately 10^{-5} W) red He–Ne laser beam at 632.8 nm. A beam chopper, lock-in amplifier, red interference filter and photomultiplier tube were used for signal detection and rejection of stray light. Even at this low power level it appeared that continuous monitoring with red light contributed to the thermal fading rate for the very slow decay at the lower temperatures (e.g. below 70 °C). To avoid this problem the diffraction efficiency was only monitored at intervals during the prolonged decays.

Heating the sample in open air was a major problem because of the spurious changes in the optical paths produced by thermal convection. As a consequence, multiple shifted gratings are written which result in higher harmonic contributions and low saturation diffraction efficiencies. A vacuum chamber was built in order to carry out all optical and thermal experiments in a static vacuum of about 10^{-2} Torr. The use of this chamber resulted in smooth (noiseless) recordings, much higher saturation values and a substantial improvement in the reproducibility.

Of particular interest is that, in the samples erased in air at temperatures above RT (in the presence of convection), the decay curves frequently showed a late-stage decay which was faster than the intermediate stages. Since this feature does not exist with the sample heated in vacuum, it is thought that the rapid final stage is an artefact of overlapping gratings formed by the distortions arising from the convection currents in the air.

The first method used was to set the sample temperature and to maintain it within better than 0.5 °C. A grating was then written with the green laser beams and the intensity monitored until the red diffraction approached a maximum value. The time dependence of the optical or thermal erasure was then recorded. The optical erasure was made with incoherent white light coming from a microscope illuminating system. Total grating erasure was observed by optical erasing. Thermal erasure proceeded much more slowly and, although total erasure was recorded at high temperatures, this was not possible in a reasonable period at lower temperatures. To ensure equivalent starting conditions before each experiment the sample was thermally cycled to above 250 °C to provide a 'fresh' sample. Reproducibility of the decay rates confirmed that this approach is effective.

The second method was to write a grating at 50 °C and then to record the diffraction efficiency whilst heating the sample at a constant rate of 2 °C min^{-1}.

3. Optical erasure

In all the sets of measurements at constant temperature the decay of the diffracted signal during optical erasure was not a simple exponential function with time. When carrying out the experiments in open air, three decay stages were often observed. The fact that the decay rate of the last stage (stage 3) is higher than that of stage 2 has been observed by other workers and considered 'anomalous'. However, when using the vacuum chamber described above, stage 3 was not present and the data were readily described as a summation of a fast (A1) and a slow (A2) exponential decays as shown in figure 1. The Arrhenius plots for these decay rates are shown in figure 2. Within experimental error the two stages proceed with the same activation energy of 0.15 ± 0.01 eV. The non-exponential behaviour might partly be attributed to a geometrical shadow effect (self-absorption) as pointed out by Baquedano *et al* (1987). The absorption coefficient of our sample was about 7 cm^{-1} at 514 nm, and this produces a noticeable deviation from simple exponential decays. However, no attempt was made to apply such an analysis since the activation energy of both components turned out to be the same.

4. Thermal erasure

Thermal erasure of the gratings was carried out via two alternative ways. One procedure was heating the sample from 50 to 165 °C at a constant rate while monitoring the

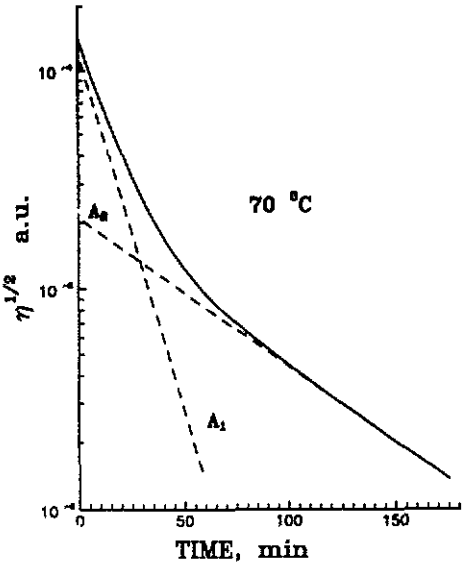

Figure 1. Optical erasure of a grating at a constant 70 °C (——) where the square root of the diffracted signal has been plotted as a function of time: – – –, the two exponential components into which the full curve can be decomposed.

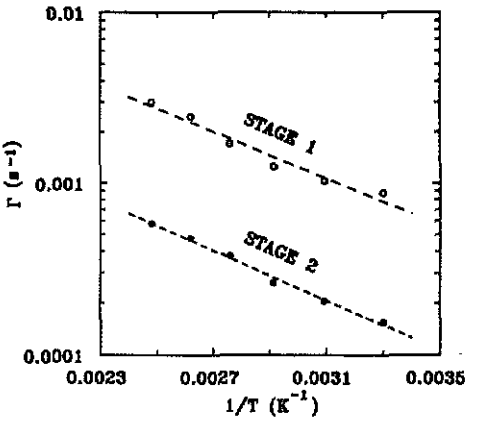

Figure 2. Arrhenius plot for decay rates Γ of the two component stages of optical erasure of a photorefractive diffraction grating in $LiNbO_3$.

diffraction efficiency. Aside from providing an alternative route to determine activation energies, this provides a direct picture of the main decay steps. A second method was measuring diffraction efficiency decay curves at constant temperature, within the range 50–165 °C. This method should give more accurate activation energies values. The data taken below 90 °C are not shown since these measurements were not made in vacuum and are considered not reliable as mentioned in section 2.

4.1. Heating at a constant rate

The data of the form shown in figure 3, curve a, describe the diffraction efficiency as a function of temperature for a grating recorded at 50 °C with a diffraction efficiency of about 25%. In order to obtain reproducible values it was necessary to form a saturated grating at 50 °C. This was only feasible with the sample in the vacuum chamber. At first sight, the main decay step appears between 130 and 140 °C. With more detailed analysis the rapidly changing slope near 135 °C indicates that more than one process is taking place. If the sample is then cooled from 165 to 50 °C and homogeneously illuminated with white light for about 8 h, a small percentage (1%) of the initial diffraction efficiency is recovered (*developing process*). This strongly supports the argument that ion migration has taken place during heating, but doubts still remain whether partial electron detrapping has proceeded at the same time. In such a case the measured activation energy would result from a mixture of both processes.

In order to investigate the decay of the developed grating, the sample was heated again until the developed signal faded out. This decay has been plotted in figure 3(*b*) with an appropriate scale factor for comparison purposes. It is seen to proceed at lower temperatures and without the sharp slope change of the first decay, indicating differences

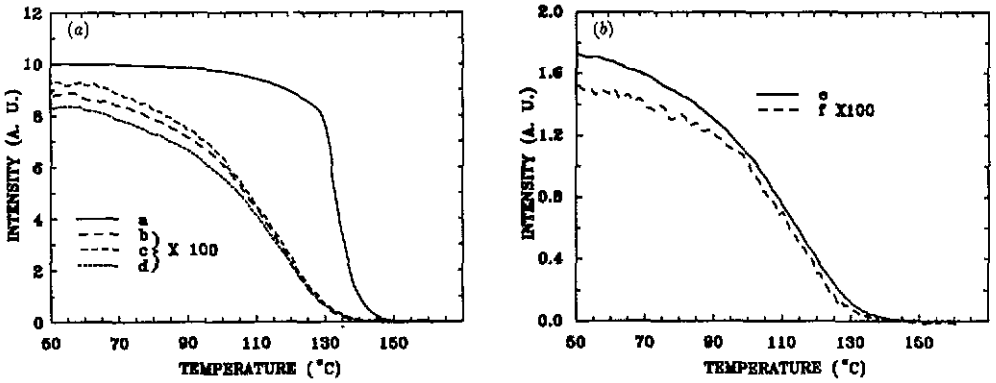

Figure 3. Thermal erasure, monitored by detecting the diffracted intensity, by heating at a constant rate of 2 °C min^{-1}: curve a, grating recorded at 50 °C up to 25% diffraction efficiency; curve b, grating developed after run a by 8 h of homogeneous illumination with white light at 50 °C; curve c, same curve as b after run b; curve d, same as curve b after run c; curve e, grating recorded at 50 °C up to 2% diffraction efficiency; curve f, same as curve b after run e).

in the physical processes taking place during the decays. On the other hand, if the process is repeated by cooling the sample to 50 °C and illuminating it again with white light, for about 8 h, a diffracted signal of the same magnitude as that of the first developed grating (1% of the original signal induced by the light beams) is recovered. Four of these cycles were carried out, the developed signal being the same in all the cases. The decay steps of the first three are plotted as figure 3, curves c and d. Within experimental error, curves b–d are seen to be the same.

When thermal erasure was carried out on a grating recorded at 50 °C with a low diffraction efficiency (about 2%) (figure 3, curve e), the thermal decay turned out to be the same as that of the developed grating (figure 3, curve f). In fact, curves b–f look like the slow decay exhibited by curve a (when magnified), up to the region of rapid decay.

4.2. Time dependence at constant temperature

The time dependence at constant temperature of the thermal erasure of the photorefractive grating was somewhat more complex and slower than that of the optically driven decay. Figure 4 shows a semilogarithmic plot of the square root $\eta^{1/2}$ of the diffraction efficiency at 150 °C, and a non-exponential dependence is clearly observed. By successive subtractions of the lowest linear section in the semilogarithmic plot (i.e. the slowest exponential component), up to four exponential components can be obtained. The obvious presence of overlap makes the fitting process uncertain to some extent; however, these components appear to be present in all data taken within the 90–165 °C range, and also in the preliminary data from 50 to 130 °C. The activation energies and pre-exponential factors for each component, obtained from the temperature dependence of the decay constants (see equation (1) in section 5), are slightly different. They fall within the ranges 0.85–0.95 eV and 10^8–10^9 s^{-1} respectively. Figure 5 illustrates the Arrhenius plot for the initial slopes of the decay curves, which give data which are scattered less than those obtained from the fittings. This gives an activation energy of 0.90 eV and a pre-exponential factor of 8.6×10^8 s^{-1}.

It should be mentioned that, when recording at temperatures above 180 °C transient effects were observed, including decreases to zero diffraction efficiency, followed by a

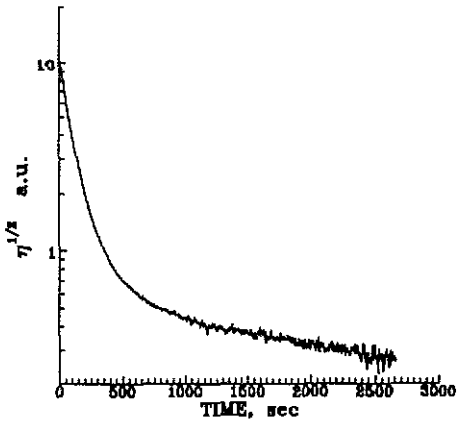

Figure 4. Thermal decay of a grating at a constant 150 °C where the square root of the diffracted signal has been plotted as a function of time.

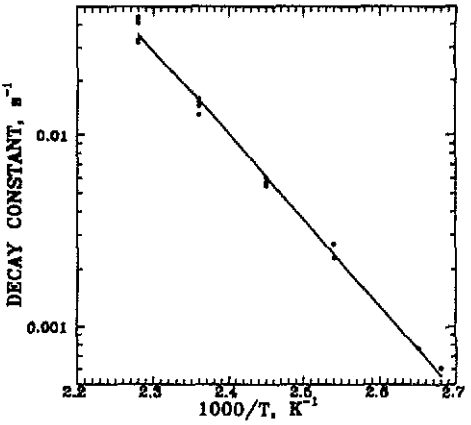

Figure 5. Arrhenius plot for decay rates during thermal erasure. To obtain the decay rates, the initial slopes of the decay curves have been taken.

signal increase. These effects are at present being studied and a full description of them will be presented elsewhere.

5. Discussion

Following the paper of Vormann *et al* (1981), it is generally accepted that photorefractive fixing in $LiNbO_3$ is mainly produced by proton migration induced by the grating space-charge field. As a consequence of the results presented above, we should add that, for fixing below 170 °C, protons are the only mobile entities, whilst electrons remain trapped during the process. This conclusion follows from our data, and from the recent fixing model put forward by Carrascosa and Agulló-López (1990). The advantage of this model is that it takes into account, simultaneously, contributions from electron detrapping and proton migration during thermal erasure. According to the model, during thermal erasure at constant high temperature (at which protons and electrons are mobile), the diffraction efficiency should decrease to zero and then increase again. This prediction has also been observed in the experiments that we have performed at temperatures above 180 °C, but there was no sign of it within the main range of temperatures used in this paper (i.e. 50–165 °C). Although protons may associate with a range of defect sites and hence show several related values of migration energy, the overall conclusion is that there is only one moving entity operating below 180 °C. Since protons have proved to be mobile below 180 °C, one may therefore conclude that electrons are mobile only at higher temperatures.

The above statement is further supported by the fact that the developed grating exhibits about 1% of the original diffraction efficiency of the grating recorded at 50 °C. Within the experimental error, this is the value predicted by all current models under the assumption that the donor grating does not suffer electron detrapping and is fully compensated by a matched proton grating. Also in agreement with this view is the conclusion, drawn from the review of Kovács and Polgár (1989) on the conductivity of $LiNbO_3$, that the conductivity is proportional to the proton concentration within the range considered here. Obviously, in other crystals, such as strongly reduced crystals

which show a lower activation energy (0.7 eV (Jösch *et al* 1978)), electron detrapping may occur at lower temperatures with the consequent mixing of electronic and protonic processes.

The complete recovery of the signal of a developed–erased grating also indicates a full compensation of the initial donor grating by the proton grating. Hence a deep proton grating with the same modulation factor as the electronic grating is produced during the fixing process. Since one developing–annealing cycle removes only less than 1% of this deep grating, the developing–annealing–developing process can be repeated several times, as shown in figure 3, without appreciable change in the developed signal. This finding provides a satisfactory explanation of the memory 'refreshment' effect of a fixed hologram. This has previously been reported by other workers as a means to increase substantially the storage time of fixed information.

Therefore, by annealing at temperatures below 165 °C, experimental determination of parameters (activation energy and pre-exponential factor) for proton migration is accessible, without overlapping with electronic contributions. The determination of electron-detrapping parameters should be possible at higher temperatures and work is in progress in this direction.

Let us consider the time dependences at constant temperature (figure 4) within this scheme. For only proton migration, the model of Carrascosa and Agulló-López (1990) predicts a simple exponential growth of the protonic grating to compensate the electronic grating, proceeding as a saturating process. Taking into account that the contribution of the proton diffusion is much smaller than the field-driven term, the square root of the diffraction efficiency should exhibit an exponential decay, i.e. $\sqrt{\eta} \propto \exp(-\Gamma t)$, where

$$\Gamma = (e^2 HD/\varepsilon k_B T) \exp(-\mathscr{E}_A/k_B T). \tag{1}$$

In this equation, e is the electron charge, ε is the dielectric constant, k_B is Boltzmann's constant, T is the absolute temperature, H is the proton concentration, D is the proton diffusion coefficient and $\mathscr{E}_A$ is the activation energy for proton migration. However, the observed decay curves (figure 4) are clearly non-exponential. As in the case of the knee in figure 3, curve a, this is an indication that further processes, more complex than discussed so far, are taking place. Moreover, the thermal decays shown in curves a and e in figure 3 are assumed to proceed via compensation of the donor grating, only by proton migration, and those decays shown in curves b–d and f in figure 3 are produced by proton migration out of the developed (slightly uncompensated) proton gratings. Therefore, curve a should show the same trend as the other four.

A reasonable explanation for this behaviour is the occurrence of different proton sites with different detrapping energies. In fact, Bollmann and Stöhr (1977) have explained their conductivity data in terms of two different OH-sites, one defect being a substitution for an O^{2-} ion, and the other being an interstitial. These two proton sites are assumed to be the origin of the two slightly different activation energies for conductivity (1.13 and 1.08 eV) and infrared absorption bands (2.875 and 2.865 μm). Other impurities also appear to affect protonic conductivity (Kovács and Polgár 1989), resulting in a rather wide range of activation energies as quoted in section 1. Figure 3 can be understood if the concentration of one type of proton site is very low, and this site generates the lower activation energy. Such proton traps would be responsible for the low-temperature stages of all the curves. The high concentration of the second type of traps disguises this fact in the case of curve a. Thermal detrapping of non-photorefractive electron traps (shallow, very low concentration traps) may also affect the shape of these curves.

Upon illumination, the gratings are actually destroyed, as opposed to the thermal case, in which the gratings are only ionically compensated. The presence of two exponential decays for optical erasure suggests that two active species are simultaneously contributing to the photorefractive process, according to theoretical predictions by Carrascosa and Agulló-López (1986), and experimental results for BSO and BGO (Baquedano *et al* 1989). No corrections have been discussed to compensate for the geometrical shadowing effects from self-absorption (Baquedano *et al* 1987). If self-absorption is introduced, then one expects that the actual decays appear to be closer to a single exponential. On the other hand, the description of the two exponential components by a single activation energy suggests that the dominant transport mechanism is by electron or polaron diffusion (hopping). The low value of the activation energy, 0.15 eV, is consistent with earlier ideas on polaron diffusion by Zylberstejn (1976). Variations in quoted values may relate to defect and trace impurity conditions within a particular crystal, or failure to appreciate that the process is not of a single-stage nature.

Acknowledgments

We are grateful to the Ministerio de Educación y Ciencia for financial assistance to PDT for this collaboration. Fruitful discussions with F Agulló-López and F Jaque are also acknowledged. This work was partially supported by Comisión Interministerial de Ciencia y Tecnología under grant TIC100/88/12781.00 and Fundación Ramón Areces.

References

Amodei J J and Staebler D L 1971 *Appl. Phys. Lett.* **18** 540
—— 1972a *RCA Rev.* **33** 71
—— 1972b *Ferroelectrics* **3** 107
Anghert N B, Pashkov V A and Solov'yeva N M 1972 *Zh. Eksp. Teor. Fiz.* **26** 1666–72
Ashkin A, Boyd G D, Dziedsic J M, Smith R G, Ballmann A A, Levinstein J J and Nassau K 1966 *Appl. Phys. Lett.* **9** 72
Balsa D F and Bobyl A V 1985 *Sov. Phys.–Solid State* **27** 313–6
Baquedano J, Carrascosa M, Arizmendi L and Cabrera J M 1987 *J. Opt. Soc. Am.* B **4** 309
Baquedano J, Contreras L, Diéguez E and Cabrera J M 1989 *J. Appl. Phys.* **66** 5146–50
Barkan B, Baskin E M and Entin M V 1980 *Phys. Status Solidi* a **59** K97
Belabaev K G, Markov V B and Odulov S G 1976 *Ukr. Fiz. Zh.* **21** 1820
Bollmann W and Stöhr H J 1977 *Phys. Status Solidi* a **39** 477–84
Carrascosa M and Agulló-López F 1986 *IEEE J. Quantum Electron.* **QE-22** 1369–75
—— 1990 *J. Opt. Soc. Am.* B **7** 2317–22
Chen F S, Macchia Y T and Fraser D V 1968 *Appl. Phys. Lett.* **13** 223–5
Hertel P, Ringhofer K H and Sommerfeldt R 1987 *Phys. Status Solidi* a **104** 855
Jösch W, Munser R, Ruppel W and Würfel P 1978 *Ferroelecticity* **21** 623–5
Kovács L and Fölvari I 1989 Properties of Lithium Niobate *Datareview EMIS* (London: INSPEC) ch 6
Kovács L and Polgár K 1989 Properties of Lithium Niobate *Datareview EMIS* (London: INSPEC) ch 4
Krätzig E and Orlowsky R 1980 *Ferroelectrics* **27** 241–4
Ohmori Y, Yamaguchi M, Yoshino K and Inuishi Y 1976 *Japan. J. Appl. Phys.* **15** 2263–4
Pashkov V A, Solov'yeva N M and Anghert N B 1979 *Fiz. Tverd. Tela* **21** 92–8, 1879–82
Vormann H, Weber G, Kapphan S and Krätzig E 1981 *Solid State Commun.* **40** 543
Zylberstejn A 1976 *Appl. Phys. Lett.* **29** 778